Commun. Comput. Chem doi: 10.4208/cicc.2017.v5.n4.2

REGULAR ARTICLE

Theoretical Treatment of Ultrafast Decay of Excited Vibronic States in the Improved Adiabatic Approximation

Jian Lei, Rongxing He*

Key Laboratory of Luminescence and Real-Time Analytical Chemistry (Southwest University), Ministry of Education, College of Chemistry and Chemical Engineering, Southwest University, Chongqing 400715, China.

Received15 Nov. 2017; Accepted (in revised version) 25 Dec. 2017

Abstract: In the present paper, the non-radiative transition $S_1 \rightarrow S_0$ of pyrazine was investigated by employing the improved Born-Oppenheimer adiabatic approximation, in which the conical intersection is shown to be avoided. Vibrational frequencies, normal coordinates, and non-adiabatic coupling matrix elements were obtained by *ab initio* quantum chemical methods. Calculated rate constants of internal conversion $S_1 \rightarrow S_0$ are $\tau_{(\nu=0)}$ =61.7 ps and $\tau_{(\nu=1)}$ =61.2 ps in good agreement with the experimental findings.

Keywords: Pyrazine; Born-Oppenheimer approximation; internal conversion; DFT

1. Introduction

Pyrazine is a diazine molecule, and its electronic structures, ultraviolet absorption spectra and internal conversions have been studied theoretically and experimentally over half a century.[1-4] The electronic spectroscopy and ultrafast dynamical processes of other diazine molecules such as pyrimidine and pyridazine have also been a very interesting subject due to its rich excited-state dynamical and photochemical properties.[5-8] Substituting a pair of nitrogen atoms for carbon ones at the *para*-position in the benzene molecule, pyrazine has a different electronic structure from benzene. As a symmetrical molecule with point group D_{2h} , the first excited state S_1 of pyrazine has a $n\pi^*$ electronic configuration.

Pyrazine molecule has been studied by both theoretical simulations and experimental

^{*} Corresponding authors. *E-mail address:* herx@swu.edu.cn http://www.global-sci.org/cicc

measurements for its low-lying excited states with applications of photophysics and photochemistry. Internal conversion process of pyrazine is described by Domcke and his co-workers through *ab initio* calculations which combined with mathematical models in the 1980s,[9] Domcke et al. proposed an ultrafast internal conversion after S₂ state excitation through conical intersection,[10-13] and the corresponding lifetime was estimated by *ab initio* calculations to be about 20fs.[14] Knee firstly determined experimental results for S₁ state lifetime to be about 110 ps for the vibrationless excitation,[15] and about 100 ps for the vibrationally excited S₁ state, reported by Suzuki.[16, 17] V. Stert[18] The results show that the lifetime of S₂ state due to internal conversion to the lower electronic states was about 20 fs.

Since the development of femtosecond lasers and their application to photochemistry and photophysics, the pump-probe experiments have become a powerful technique to study the femtosecond time-resolved spectroscopies and femtosecond dynamical processes. It is due to its numerous dynamical processes in biology and chemistry and physics are in femtosecond time scale. A main purpose of this paper is to analyze the experimental results of ultrafast dynamical processes by using the improved Born-Oppenheimer adiabatic approximation. Therefore, the experimental results of Suzuki's group[16, 17] will be analyzed and the improved Born-Oppenheimer adiabatic approximation will be employed to calculate the lifetime of vibronic states of pyrazine.

2. Computational methods and theoretical details

The improved Born-Oppenheimer adiabatic approximation is briefly described in the following.[19] Notice that the molecular Schrödinger equation is given by

$$\hat{H}\psi(Q,r) = \hat{E}\psi(Q,r)\,,\tag{1}$$

where

$$\hat{H} = \hat{T}_n + \hat{T}_e + V(Q, r) = \hat{T}_n + \hat{H}_e,$$
 (2)

and

$$\hat{H}_{e}\Phi_{a}(Q,r) = U_{a}(Q)\Phi_{a}(Q,r),$$
 (3)

We shall let

$$\psi(Q,r) = \sum_{a} \Theta_{a}(Q) \Phi_{a}(Q,r) \tag{4}$$

where

$$\hat{T}_{n}\Theta_{a}\Phi_{a} = \Phi_{a}\hat{T}_{n}\Theta_{a} + \Theta_{a}\hat{T}_{n}\Phi_{a} - \hbar^{2}\sum_{i}\frac{\partial\Theta_{a}}{\partial Q_{i}}\frac{\partial\Phi_{a}}{\partial Q_{i}},$$
(5)

Substituting Eqs.(4) and (5) into Eq.(1) yields

$$\sum_{a} (\Phi_{a} \hat{T}_{n} \Theta_{a} + \Theta_{a} \hat{T}_{n} \Phi_{a} - \hbar^{2} \sum_{i} \frac{\partial \Theta_{a}}{\partial Q_{i}} \frac{\partial \Phi_{a}}{\partial Q_{i}} + \Theta_{a} \hat{H}_{e} \Phi_{a}) = \sum_{a} E \Theta_{a} \Phi_{a} , \qquad (6)$$

and

$$\hat{T}_{n}\Theta_{b} + U_{b}\Theta_{b} + \left\langle \Phi_{b} \middle| \hat{T}_{n} \middle| \Phi_{b} \right\rangle \Theta_{b} + \sum_{a}^{a \neq b} \left(\Theta_{a} \left\langle \Phi_{b} \middle| \hat{T}_{n} \middle| \Phi_{a} \right\rangle \right)
- \hbar^{2} \sum_{i} \left\langle \Phi_{b} \middle| \frac{\partial \Phi_{a}}{\partial Q_{i}} \right\rangle \frac{\partial \Theta_{a}}{\partial Q_{i}} = E\Theta_{b}$$
(7)

In the improved adiabatic approximation, we obtain

$$(\hat{\mathbf{T}}_{\mathbf{p}} + \overline{\mathbf{U}}_{\mathbf{p}})\boldsymbol{\Theta}_{\mathbf{p}} = \mathbf{E}\boldsymbol{\Theta}_{\mathbf{p}}, \tag{8}$$

where

$$\overline{\mathbf{U}}_{b} = \mathbf{U}_{b} + \left\langle \Phi_{b} \middle| \hat{\mathbf{T}}_{n} \middle| \Phi_{b} \right\rangle, \tag{9}$$

and U_b denotes the conventional adiabatic approximation, while \overline{U}_b denotes the improved adiabatic approximation.

Notice that

$$\left\langle \Phi_{a} \middle| \hat{T}_{n} \middle| \Phi_{a} \right\rangle = -\sum_{i} \frac{\hbar^{2}}{2} \left\langle \Phi_{a} \middle| \frac{\partial^{2}}{\partial Q_{i}^{2}} \middle| \Phi_{a} \right\rangle$$

$$= -\sum_{i} \frac{\hbar^{2}}{2} \left\langle \Phi_{a} \middle| \frac{\partial}{\partial Q_{i}} \sum_{b} \middle| \Phi_{b} \right\rangle \left\langle \Phi_{b} \middle| \frac{\partial}{\partial Q_{i}} \middle| \Phi_{a} \right\rangle, \tag{10}$$

$$= \sum_{b} \sum_{i} \frac{\hbar^{2}}{2} \frac{\left| \left\langle \Phi_{a} \middle| \frac{\partial V}{\partial Q_{i}} \middle| \Phi_{b} \right\rangle \middle|^{2}}{\left(U_{b} - U_{a}\right)^{2}} \ge 0$$

Based on the discussion of improved adiabatic approximation the internal conversion from electronic state b to a, for the vibronic state av can be expressed as

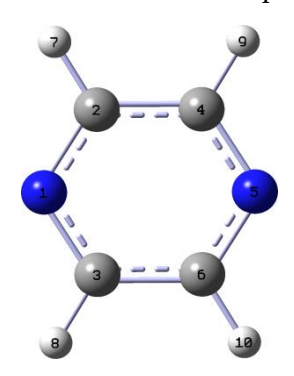


Figure 1: Numbering of atoms for pyrazine optimized by DFT/B3LYP.

$$\mathbf{W}_{av} = \frac{2\pi}{\hbar^2} \sum_{v} \left| \left\langle \Psi_{bv'} \middle| \hat{\mathbf{H}}'_{BO} \middle| \Psi_{av} \right\rangle \right|^2 \delta(\omega_{bv',av} - \omega), \tag{11}$$

where

$$\left\langle \Psi_{bv'} \middle| \hat{H}'_{BO} \middle| \Psi_{av} \right\rangle = -\frac{\hbar^2}{2} \sum_{i} \Theta_{bv'} \left\langle \left| -\hbar^2 \left\langle \Phi_{b} \middle| \frac{\partial \Phi_{a}}{\partial Q_{i}} \cdot \frac{\partial}{\partial Q_{i}} + \frac{1}{2} \frac{\partial^2 \Phi_{b}}{\partial Q_{i}^2} \right\rangle \middle| \Theta_{av} \right\rangle, \tag{12}$$

Here the equation is based on the improved adiabatic approximation.

Notice that the conical intersection is based on the relation U_a = U_b in the conventional adiabatic approximation. In this paper, we calculate the internal conversion based on the break-down of the improved adiabatic approximation. For example, if we are concerned with the crossing between the electronic states a and b, we obtain $\overline{U}_a = \overline{U}_b$. In the improved Born-Oppenheimer adiabatic approximation this can approximately happen when other electronic states are very far away from a and b states.

To investigate the equilibrium geometries and all 24 normal-mode frequencies of relevant electronic states of pyrazine, Gaussian09[20] program package was employed to calculate the electronic structures of the ground state S₀ and the first singlet excited state S₁. The numbering of atoms for pyrazine optimized by DFT/B3LYP is shown in **Figure 1**. On one hand, the geometries of the ground state S₀ of pyrazine in vapors was optimized at the MP2, B3LYP and CASSCF level with the 6-311++G** basis set. On the other hand, we have employed TD-B3LYP and CASSCF approaching with the same basis set to calculate the excited state S₁. The stability of all the optimized geometries is checked by the frequency simulation which the normal modes and the harmonic vibrational frequencies of pyrazine in the two electronic states are all obtained.

3. Results and discussion

We optimized the geometrical parameters of pyrazine in its electronic ground state and the excited state by using DFT and *ab initio* calculation shown in **Table 1**, together with the experimental and other theoretical data.[21-23] In this work, the B3LYP, MP2 and CASSCF were applied to optimize the equilibrium geometry of the ground state S₀, and the TD-B3LYP and CASSCF were used to optimize the equilibrium geometry of excited state.

From **Table 1**, the present CASSCF results are indeed in good agreement with the previous computational and experimental data, revealing accurate geometries for the ground state and excited states. The optimized results for the first excited state S_1 in the **Table 1** indicate that all the C-C bonds and C-N bonds of S_1 state are longer compared with those of the ground state. It means the molecular ring is expanded. For example, the C-C bond of S_0 calculated by CASSCF is 1.395 Å, but that of S_1 at the same level is 1.423 Å. It is obvious that S_1 is an $n\pi^*$ state, so the electronic transition of the first excited state makes the

result understandable, indicating that an n-type electron located on nitrogen atom is transferred to the anti-bonding π^* orbital on the pyrazine ring when the excitation takes place. This leads to the longer bonds because of the increase of charge located on the anti-bonding orbital.

Table 1. The optimized geometries of pyrazine in its ground state (S_0 (1A_g)), the first excited state (S_1 ($^1B_{3u}$ $n\pi^*$)). The bond length (r) is in Å and the angle (θ) in degree.

method	sym	r(C-N)	R(C-C)	r(C-H)	θ CNC	θ NCC	θ NCH	
S ₀ ¹ A _g								
$EXP^{a)}$	D_{2h}	1.338	1.397	1.083	115.7	122.2	117.9	
B3LYPb)	D_{2h}	1.335	1.395	1.086	116.0	122.0	117.2	
CASSCF ^{b)}	D_{2h}	1.329	1.395	1.075	116.1	122.0	117.2	
B3LYP	D_{2h}	1.335	1.396	1.086	116.1	121.9	117.1	
CAMB3LYP	D_{2h}	1.328	1.389	1.085	116.2	121.9	117.2	
MP2	D_{2h}	1.317	1.386	1.075	116.6	121.7	117.5	
HF	D_{2h}	1.317	1.386	1.075	116.6	121.7	117.5	
CAS	D_{2h}	1.330	1.395	1.075	116.0	122.0	117.3	
S ₁ ¹ B _{3u}								
TD-B3LYP ^{b)}	D_{2h}	1.343	1.396	1.084	120.0	120.0	120.5	
CASSCF ^b	D_{2h}	1.353	1.383	1.072	119.6	120.2	119.5	
B3LYP	D_{2h}	1.343	1.396	1.084	120.0	120.0	120.6	
CAMB3LYP	D_{2h}	1.336	1.390	1.083	120.4	119.8	120.8	
CAS	D_{2h}	1.353	1.423	1.082	119.6	120.2	119.5	

a)Ref.[22]; b) Ref.[21].

Table 2. The calculated vertical excitation energies (Δ EFC), adiabatic excitation energies (Δ Ead) and oscillator strengths, together with the experimental and previous theoretical data.

State		S ₁ (¹ B _{3u}))	
Excitation energy	ΔE_{FC}	ΔE_{ad}	f_{10}	
EXPa)	3.94	3.83	0.006	
TD-B3LYPb)	3.94	3.83	0.707	
CASSCFb)	4.87	4.72	-	
CIS ^{b)}	4.88	-	0.009	
TD-B3LYP	3.71	3.83	0.706	
CASSCF	4.56	4.42	-	
CIS	4.88	-	0.010	

According to the molecular orbital maps and excitation coefficients calculated by TD-DFT shown in **Figure 2** and **Table 2**, the present CASSCF calculations make clear that the results of the first excited state S₁ are mainly from the excitation from HOMO orbital to LUMO orbital which the non-bonding electron enters the C-N-bonding or C-C-anti-bonding orbital, leading to the ring deformation.

Vibrational frequencies of all 24 modes are calculated by B3LYP, HF, MP2 and CASSCF (10, 8) for S_0 and by B3LYP, CIS and CASSCF (10, 8) for S_1 with the basis set 6-311++g**. The results are shown in **Table 3**. In comparison with the experimental results[24] measured by the infrared and Raman spectroscopy, both results calculated by B3LYP and CASSCF methods are in good agreement with experiment. The 24 modes, the total symmetry modes, exhibit the differences of the frequency between the excited state and the ground state. Four modes v_{6a} , v_{1} , v_{9a} and v_{2} are significant figures for the first excited state, which explains the great changes in the inner angles of the ring account for the highest intensity of the bending mode v_{6a} . Therefore, the displaced oscillator approximation can be considered as a good approximation for calculating the non-radiative transition rate.

As shown in **Table 3**, MP2 and B3LYP provide very accurate harmonic vibrational frequencies for the ground state of pyrazine, and it is obvious that the frequencies of CASSCF and HF are slightly overestimated relative to those of MP2 and functional B3LYP. For the electronic state S_1 , the harmonic frequencies predicted by CASSCF are nearly identical. However, for the B3LYP results, it is noted that the frequencies of modes v_{6a} and v_{1} are larger than the experimental results, and the results of CIS are also higher than the theoretical and experimental data.

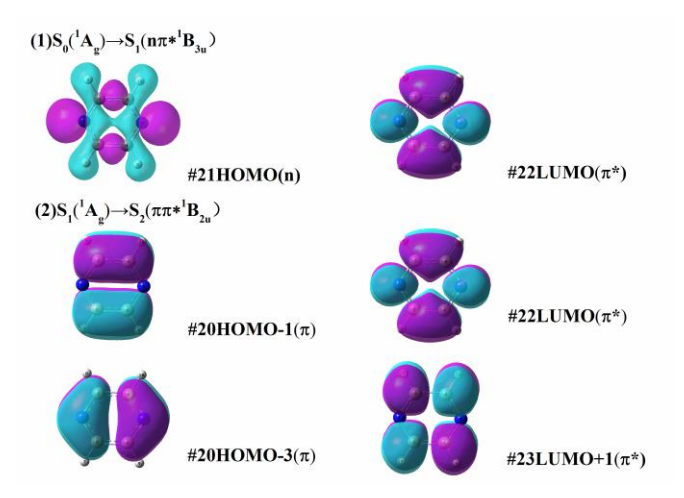


Figure 2: Frontier molecular orbital maps of pyrazine calculated by DFT/B3LYP. HOMO and HOMO-2 show the nonbonding character, HOMO-1 and HOMO-3 are π bonding, and LUMO and LUMO+1 are π^* anti-bonding excitation. (1) S₀ ($^{1}A_{g}$) \rightarrow S₁ ($^{1}n\pi^{*1}B_{3u}$) excitation. (2) S₀ ($^{1}A_{g}$) \rightarrow S₂ ($^{1}n\pi^{*1}B_{2u}$) excitation.

Table 3. Experimental and calculated vibrational frequencies (cm⁻¹) of 24 normal modes for the ground and the excited states of pyrazine.

				S_0			S ₁	
sym	Mode ^{a)}	EXPb)	B3LYP	MP2	CAS	EXP	B3LYP	CAS
ag	V6a	596	612	601	644	585	620	561
	V 1	1015	1038	1026	1073	970	1024	1007
	V9a	1230	1253	1259	1324	1104	1195	1257
	V8a	1582	1612	1613	1734	1377	1534	1589
	V_2	3055	3173	3221	3351		3195	3405
$b_{1g} \\$	V_{10a}	919	940	903	960	383	468	287
$b_{2g} \\$	V4	756	772	676	784	518	511	577
	V 5	983	979	897	997	552	810	914
b_{3g}	V ₆ b	704	720	711	758	662	688	686
	V 3	1346	1373	1372	1467	-	1295	1391
	V8b	1525	1579	1565	1663	-	-602	932
	V 7b	3040	3152	3201	3328	-	3160	3337
a_{u}	V 16a	341	347	304	388	400	432	478
	V 17a	960	988	844	1005	743	823	913
b_{1u}	V 12	1021	1035	1034	1152	-	624	925
	V18a	1136	1165	1162	1237	-	1013	1061
	V 19a	1784	1511	1505	1625	-	1390	1523
	V 13	3012	3153	3202	3331	-	3169	3341
$b_{2u} \\$	\mathbf{V}_{15}	1063	1088	1088	1133	-	1080	1138
	V 14	1149	1218	1352	1165	-	1267	1458
	V 19b	1416	1440	1442	1532	-	1357	1499
	V20b	3063	3167	3216	3346	-	3192	3400
b_{3u}	V16b	420	432	406	461	236	220	224
	V 11	785	801	778	832	898	722	710

a) v_{8a} and v_{9a} are according to Refs.[4, 11]; b) Ref.[23].

We construct harmonic potential energy surfaces from both present adiabatic S₁ and S₂ states at their corresponding equilibrium geometries. For the S₁ state, the equilibrium geometries are slightly different, but vibrational frequencies are about the same from adiabatic representations. Thus S₀ and S₁ states potential energy surfaces are completely superimposed. The reason is that the equilibrium geometry of the S₁ state is not close to conical intersection, and the vibronic coupling does not affect its minimum so much. Four

modes v_{6a} , v_{1} , v_{9a} and v_{8a} in adiabatic representation presents a quantitative description of deviation for S_{0} and S_{1} potential energy surfaces calculated from adiabatic and non-diabatic representations. This deviation represents that vibronic coupling at conical intersection may not affect S_{1} state strongly. Thus, we can use the equilibrium geometries of the calculated S_{0} , S_{1} states to estimate the Huang-Rhys factors. For mode v_{6a} , the CASSCF and B3LYP Huang-Rhys factors are 0.680 and 0.347, respectively. This indicates that the CASSCF Huang-Rhys factors are reasonable.

As the case of absorption spectra and non-radiative transition process of pyrazine, the curve crossing does not happen very often compared with the tunneling events. The reason is that the Born-Oppenheimer approximation works well in the treatment of absorption and emission spectra and their non-adiabatic transition. The formalism described in the theory section allows the calculation of the rate constants of internal conversion between various singlet electronic states using vibronic coupling. The S₁→S₀ transition rate constant of non-radiative relaxation pathways was calculated, and the results are presented in Table 4. Once the improved Born-Oppenheimer coupling matrix elements are obtained by collecting calculated vibrational frequencies and Franck-Condon factors, the total transition rate constant of internal conversion was estimated by using the saddle point method. It was noticed that additional approximations concerning displaced oscillator and the improved Born-Oppenheimer adiabatic approximation have also been taken into account in generating nuclear correlation functions. The single level rate constant of the internal conversion $S_1 \rightarrow S_0$ of pyrazine is determined by the following factors: 1) energy gap between the two electronic states ω_{ab} ; 2) frequency of the promoting mode ω_P ; 3)Huang-Rhys factors S_i and frequencies ωi of the totally symmetric displaced accepting modes; 4)vibronic coupling. It should be mentioned again that the elements in the dipole terms, including vibronic coupling coefficients and transition dipole moments between different excited states, depend subtly on the active space as well as on the number of states averaged in the CASSCF calculations.

Table 4. Non-radiative transition rate constants (W) and lifetimes (τ) of the $S_1 \rightarrow S_0$ and $S_2 \rightarrow S_1$.

	$S_1 \rightarrow S_0$
it*/fs	2.262×10 ⁴
$G(t^*)$	1.008
$W(0)/{ m fs}^{-1}$	1.621×10 ⁻⁵
$W(1)/fs^{-1}$	1.634×10 ⁻⁵
$\tau(0)/fs$	6.170×10 ⁴
τ(1)/fs	6.120×10 ⁴

Summarized in **Table 4**, this method estimated the lifetime of $S_1 \rightarrow S_0$ is $\tau_{v_k} = 61.7$ ps and $\tau_{v_{k=0}} = 61.2$ ps, which agrees with experimental order of magnitude $\tau \sim 100$ ps. Therefore, using the improved Born-Oppenheimer adiabatic approximation to calculate the rate constant of internal conversion of the $S_1 \rightarrow S_0$ non-radiative $n\pi^*$ transition is applicable.

4. Conclusions

In this work, we calculated the rate constant of internal conversion of the $S_1 \rightarrow S_0$ non-radiative $n\pi^*$ transition by using harmonic oscillator approximation and the improved Born-Oppenheimer adiabatic approximation for pyrazine molecule. The geometries and electronic structures of the ground and the first excited state were detected using several quantum chemistry methods. By using the improved Born-Oppenheimer approximation, the calculated lifetimes of $S_1 \rightarrow S_0$ of pyrazine are in good agreement with experimental one indicating that the present model can provide an acceptable interpretation without considering the conical intersection.

Acknowledgements

This work was supported by Chongqing Municipal Natural Science Foundation (cstc2013jcyjA90015) and the Fundamental Research Funds for the Central Universities (No. XDJK2013A008).

References

- [1] M. Ito, R. Shimada, T. Kuraishi, W. Mizushima, Vibrational spectra of diazines, The Journal of Chemical Physics, 25 (1956) 597-598.
- [2] M. Ito, R. Shimada, T. Kuraishi, W. Mizushima, Ultraviolet Absorption of Pyrazine Vapor Due to $n-\pi$ Transition, The Journal of Chemical Physics, 26 (1957) 1508-1515.
- [3] F. Halverson, R.C. Hirt, Near ultraviolet solution spectra of the diazines, The Journal of Chemical Physics, 19 (1951) 711-718.
- [4] C. Woywod, W. Domcke, A.L. Sobolewski, H.J. Werner, Characterization of the S1–S2 conical intersection in pyrazine using abinitio multiconfiguration self-consistent-field and multireference configuration-interaction methods, The Journal of chemical physics, 100 (1994) 1400-1413.
- [5] J. Parkin, K. Innes, The vacuum ultraviolet spectra of pyrazine, pyrimidine, and pyridazine vapors: Part I. Spectra between 1550 Å and 2000 Å, Journal of Molecular Spectroscopy, 15 (1965) 407-434.
- [6] B.J. Cohen, H. Baba, L. Goodman, Fluorescence from Pyridazine and Pyrimidine (n, π^*) States, The Journal of Chemical Physics, 43 (1965) 2902-2903.
- [7] L. Yang, C. Zhu, J. Yu, S.H. Lin, Anharmonic Franck–Condon simulation of the absorption and fluorescence spectra for the low-lying S₁ and S₂ excited states of pyrimidine, Chemical Physics, 400 (2012) 126-136.

- [8] Y. Matsumoto, S.K. Kim, T. Suzuki, Femtosecond photoelectron imaging of pyridazine: S1 lifetime and (3s (n-1), 3p (n-1)) Rydberg state energetics, Journal of Chemical Physics, 119 (2003) 300-303.
- [9] R. Schneider, W. Domcke, S₁-S₂ Conical intersection and ultrafast S₂→ S₁ Internal conversion in pyrazine, Chemical physics letters, 150 (1988) 235-242.
- [10] M. Seel, W. Domcke, Femtosecond time-resolved ionization spectroscopy of ultrafast internalconversion dynamics in polyatomic molecules: Theory and computational studies, The Journal of chemical physics, 95 (1991) 7806-7822.
- [11] L. Seidner, G. Stock, A. Sobolewski, W. Domcke, Abinitio characterization of the S₁–S₂ conical intersection in pyrazine and calculation of spectra, The Journal of chemical physics, 96 (1992) 5298-5309.
- [12] G. Stock, W. Domcke, Femtosecond spectroscopy of ultrafast nonadiabatic excited-state dynamics on the basis of ab initio potential-energy surfaces: the S2 state of pyrazine, The Journal of Physical Chemistry, 97 (1993) 12466-12472.
- [13] G. Stock, C. Woywod, W. Domcke, T. Swinney, B.S. Hudson, Resonance Raman spectroscopy of the S1 and S2 states of pyrazine: Experiment and first principles calculation of spectra, The Journal of chemical physics, 103 (1995) 6851-6860.
- [14] G. Stock, R. Schneider, W. Domcke, Theoretical studies on the femtosecond real-time measurement of ultrafast electronic decay in polyatomic molecules, The Journal of Chemical Physics, 90 (1989) 7184-7194.
- [15] J. Knee, F. Doany, A. Zewail, Intramolecular dephasing in pyrazine: direct picosecond time resolution, Journal of Chemical Physics, 82 (1985) 1042-1043.
- [16] L. Wang, H. Kohguchi, T. Suzuki, Femtosecond time-resolved photoelectron imaging, Faraday Discuss., 113 (1999) 37-46.
- [17] T. Suzuki, Femtosecond time-resolved photoelectron imaging, Annu. Rev. Phys. Chem., 57 (2006) 555-592.
- [18] V. Stert, P. Farmanara, W. Radloff, Electron configuration changes in excited pyrazine molecules analyzed by femtosecond time-resolved photoelectron spectroscopy, Journal of Chemical Physics, 112 (2000) 4460-4464.
- [19] S. Lin, H. Eyring, Study of vibronic and born-oppenheimer couplings, Proceedings of the National Academy of Sciences, 71 (1974) 3415-3417.
- [20] M. Frisch, G. Trucks, H. Schlegel, G. Scuseria, M. Robb, J. Cheeseman Jr, J. Montgomery, T. Vreven, K. Kudin, J. Burant, Gaussian, Inc., Wallingford CT, Gaussian 09 (Revision-A. 01); Gaussian, Inc.: Pittsburgh, PA, (2009).
- [21] R. He, C. Zhu, C.-H. Chin, S.-H. Lin, Theoretical study on S1 (1B3u) state electronic structure and absorption spectrum of pyrazine, Science in China Series B: Chemistry, 51 (2008) 1166-1173.
- [22] R. He, C. Zhu, C.-H. Chin, S.H. Lin, Ab initio studies of excited electronic state S 2 of pyrazine and Franck–Condon simulation of its absorption spectrum, Chemical Physics Letters, 476 (2009) 19-24.

- [23] C.K. Lin, Y. Niu, C. Zhu, Z. Shuai, S.H. Lin, The Role of the $n\pi^*$ 1Au State in the Photoabsorption and Relaxation of Pyrazine, Chemistry-an Asian Journal, 6 (2011) 2977.
- [24] K. Innes, I. Ross, W.R. Moomaw, Electronic states of azabenzenes and azanaphthalenes: a revised and extended critical review, Journal of Molecular Spectroscopy, 132 (1988) 492-544.